AGU PUBLICATIONS
JGR
Journal of Geophysical Research: Oceans

RESEARCH ARTICLE
10.1002/2014JC010256

Key Points:
- Heat budget for southeast Pacific
- New method combines Argo and mooring data
- Advection balances air-sea and Ekman pumping

Correspondence to:
J. Holte,
jholte@whoi.edu

Citation:
Holte, J., F. Straneo, J. T. Farrar, and R. A. Weller (2014), Heat and salinity budgets at the Stratus mooring in the southeast Pacific, *J. Geophys. Res. Oceans*, *119*, 8162–8176, doi:10.1002/2014JC010256.

Received 18 JUN 2014
Accepted 5 NOV 2014
Accepted article online 8 NOV 2014
Published online 28 NOV 2014

Heat and salinity budgets at the Stratus mooring in the southeast Pacific

James Holte[1], Fiammetta Straneo[1], J. Thomas Farrar[1], and Robert A. Weller[1]

[1]Woods Hole Oceanographic Institution, Woods Hole, Massachusetts, USA

Abstract The surface layer of the southeast Pacific Ocean (SEP) requires an input of cold, fresh water to balance heat gain, and evaporation from air-sea fluxes. Models typically fail to reproduce the cool sea surface temperatures (SST) of the SEP, limiting our ability to understand the variability of this climatically important region. We estimate the annual heat budget of the SEP for the period 2004–2009, using data from the upper 250 m of the Stratus mooring, located at 85°W 20°S, and from Argo floats. The surface buoy measures meteorological conditions and air-sea fluxes; the mooring line is heavily instrumented, measuring temperature, salinity, and velocity at more than 15 depth levels. We use a new method for estimating the advective component of the heat budget that combines Argo profiles and mooring velocity data, allowing us to calculate monthly profiles of heat advection. Averaged over the 6 year study period, we estimate a cooling advective heat flux of -41 ± 29 W m^{-2}, accomplished by a combination of the mean gyre circulation, Ekman transport, and eddies. This compensates for warming fluxes of 32 ± 4 W m^{-2} due to air-sea fluxes and 7 ± 9 W m^{-2} due to vertical mixing and Ekman pumping. A salinity budget exhibits a similar balance, with advection of freshwater (-60 psu m) replenishing the freshwater lost through evaporation (47 psu m) and Ekman pumping (14 psu m).

1. Introduction

The southeast Pacific Ocean (SEP) features the world's largest and most persistent subtropical stratocumulus cloud deck, as well as some of the coolest sea surface temperatures (SSTs) of all subtropical regions. The clouds, extending from the equator to central Chile and approximately 1500 km offshore, contribute to Earth's radiation balance and climate by reflecting incoming solar radiation [*Hartmann et al.*, 1992; *Klein and Hartmann*, 1993]. Although the clouds reduce the amount of solar radiation reaching the sea surface [*Ma et al.*, 1996; *Gordon et al.*, 2000; *de Szoeke et al.*, 2012], the SEP is a region of ocean heat gain and strong freshwater loss from air-sea fluxes [*Colbo and Weller*, 2007; *Yu and Weller*, 2007]. A combination of oceanic processes must therefore maintain the cool surface layer of the SEP; these processes are difficult to reproduce in models and to diagnose in observational studies, yet crucial to predicting and understanding climate variability.

Many coupled Global Climate Models (GCMs) do not correctly reproduce the SEP's cool SSTs or the extensive stratus clouds, limiting the models' abilities to simulate Earth's climate [*Mechoso et al.*, 1995; *Boville and Gent*, 1998; *Ma et al.*, 1996; *Lin*, 2007; *de Szoeke and Xie*, 2008; *Lauer et al.*, 2010], as well as our ability to understand the mechanisms regulating the SEP. For example, all 19 coupled GCMs used in the Intergovernmental Panel on Climate Change (IPCC) Fourth Assessment Report had warm SST biases in the SEP [*Zheng et al.*, 2011]. The inability of coupled GCMs to simulate the SEP has been attributed to poor model representation of both upper ocean heat transport and the surface heat budget [*Large and Danabasoglu*, 2006; *de Szoeke et al.*, 2010; *Zheng et al.*, 2010; *Colas et al.*, 2011].

The Stratus mooring, deployed at 85°W 20°S in the SEP since 2000, provides unique observations of the entire water column as well as the meteorological conditions and air-sea fluxes. In one attempt to estimate the heat budget of the upper 250 m of the SEP from observations, *Colbo and Weller* [2007] used the first 4 years of data from the mooring. Over this period, the mooring recorded an annual net surface heat gain of approximately 44 W m^{-2}. Heat advection due to the mean geostrophic gyre circulation compensated for slightly under half of this heating. One of the key assumptions of their study was that the World Ocean Atlas historical climatology and a collection of CTD profiles could be used to estimate the horizontal temperature

gradients; these gradients were assumed invariant to calculate the mean heat advection over the entire 4 year study period. Ekman transport, Ekman pumping, and vertical mixing made negligible contributions to their budget. Thus, *Colbo and Weller* [2007] proposed that the horizontal eddy heat flux divergence accounted for the residual cooling necessary to balance the heat budget, though they could not directly estimate it. Specifically, they suggested that eddies in the SEP, which form near the coast and propagate westward [e.g., *Chaigneau and Pizarro*, 2005a; *Johnson and McTaggart*, 2010; *Chelton et al*., 2011; *Chaigneau et al*., 2011], transport cool, upwelled coastal waters offshore.

A number of recent studies, however, have suggested that eddies do not contribute to the offshore heat balance of the SEP. *Zheng et al*. [2010], using a GCM, found that the net incoming solar heat flux of 18 W m^{-2} was nearly fully balanced by the gyre circulation of upwelled cold water from the coast. *Colas et al*. [2011] found that a combination of mean circulation, with a small contribution from Ekman transport, balanced atmospheric heating of approximately 20 W m^{-2}. Both of these modeling studies reported incoming solar heat fluxes that were less than half of the flux observed by the Stratus mooring in *Colbo and Weller* [2007]. These studies, as well as *Toniazzo et al*. [2010], argued that the eddy heat flux divergence was not spatially coherent, and therefore was unlikely to contribute to the SEP's heat balance. In an observational study based on hydrographic data from cruises, Argo float profiles, drifter records, and satellite sea surface temperature fields, *Holte et al*. [2013] also found little evidence for a strong eddy heat flux in the surface layer of the SEP; within each data set, the mean eddy surface temperature anomalies were small, and of approximately equal magnitude but opposite sign for cyclonic and anticyclonic eddies.

The biased modeling results, the limited observational studies, and the inconsistencies between previous studies suggest that the SEP's heat balance remains an open question. Since *Colbo and Weller*'s [2007] study, the Stratus mooring has collected 7 additional years of data. During this period, significant trends in surface wind stress, latent heat flux, and the net heat flux have been observed (R. Weller, Variability and trends in surface meteorology and air-sea fluxes at a site off Northern Chile, submitted to *Journal of Climate*, 2014). At the same time, the Argo array of profiling floats can now provide information about the horizontal ocean structure near the Stratus mooring.

In this study, we use a novel method combining Stratus mooring data with Argo profiles to examine the annual heat balance for the upper 250 m of the Stratus mooring record; we want to understand how the SEP maintains relatively cool surface temperatures despite such strong surface forcing. Whereas *Colbo and Weller* [2007] relied on the World Ocean Atlas historical climatology to estimate the meridional temperature gradient and on a collection of CTD and XBT profiles to estimate the zonal temperature gradient, we use Argo profiles to estimate the monthly horizontal temperature gradients near the Stratus mooring. These gradients, as well as the velocity measurements from the mooring, are used to calculate the horizontal heat advection. Because we estimate profiles of the horizontal heat advection using monthly fields, our advection term includes contributions from the gyre circulation, Ekman transport, and eddies. The residual of the budget includes all processes with time scales that are not resolved by our monthly data. The budget is evaluated for 2004–2009.

Averaged over the 6 year study period, we find that a cool advective heat flux of -41 ± 29 W m^{-2} (annual mean $\pm$ standard error) compensates for a warming air-sea heat flux of 32 ± 4 W m^{-2}, as well as a warming flux of 7 ± 9 W m^{-2} due to vertical mixing and Ekman pumping. Although the residual of our budget is small (2 ± 29 W m^{-2}), the advection term is highly variable year to year, likely due to the passage of numerous eddies as well as to the 2007–2008 La Niña; this implies that a long data record is crucial to resolving and understanding the heat budget of the SEP. A salinity budget exhibits a similar balance, with advection of freshwater replenishing the freshwater lost through evaporation and Ekman pumping. The discrepancies between our study and *Colbo and Weller* [2007] are considered in the discussion, as well as the implications of our results to understanding the interannual variability of the SEP and to observing and modeling the SEP.

The rest of the paper is organized as follows: Section 2 describes the heat budget equation and outlines the Stratus mooring and Argo data used to evaluate it, as well as various remote-sensing products used to supplement the in situ observations. Section 3 describes the results of the heat budget calculation. Section 4 outlines the salinity budget. The findings are summarized and discussed in section 5.

2. Methodology and Data

We examine the annual heat balance for the Stratus mooring using the same formulation of the heat equation as *Colbo and Weller* [2007]:

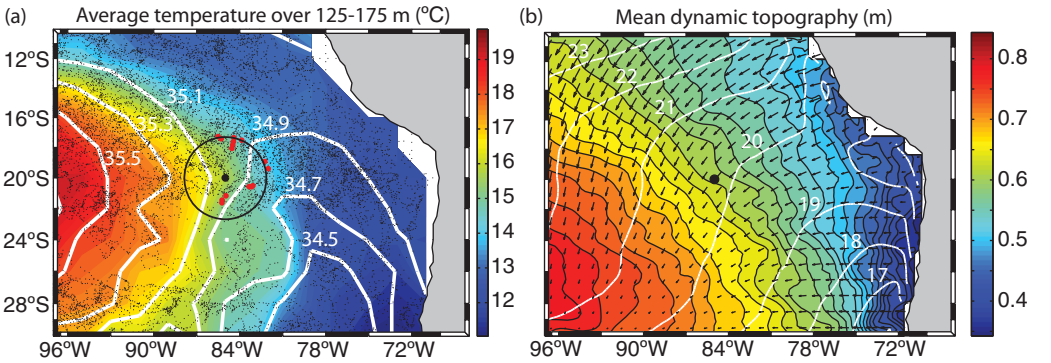

Figure 1. (a) Average temperature (color) and salinity (white contours) between 125 and 175 m generated from 12,628 Argo profiles. The temperature and salinity fields are averaged into 2° bins. The Stratus mooring (large black dot) is located at 85°W 20°S. The black circle surrounding the mooring represents a range of 300 km from the mooring. The small black dots denote the locations of the Argo profiles collected between 13 February 2003 and 1 June 2013. The 15 Argo profiles closest to the Stratus mooring from March 2008 are marked by red dots. (b) Mean dynamic topography (color) and Ekman transport (arrows) over the Argo time period. The mean SST contours (white contours) and the location of the Stratus mooring (black dot) are also plotted.

$$\int_0^{1\ year}\int_{z_o}^{o}\frac{\partial T}{\partial t}\,dz dt=\int_0^{1\ year}\left(\frac{Q_{net}}{c_p\rho_o}-\int_{z_o}^{0}\left(\vec{u}\cdot\nabla T+w_E\frac{dT}{dz}+\frac{\partial\overline{u'T'}}{\partial x}+\frac{\partial\overline{v'T'}}{\partial y}\right)dz-\kappa_V\frac{dT}{dz}\bigg|_{z=z_o}\right)dt \qquad (1)$$

where T is the temperature, Q_{net} is the net surface heat flux, c_p is the specific heat of seawater at constant pressure, ρ_o is the density, u is the velocity, w_E is the Ekman pumping velocity, $\overline{u'T'}$ and $\overline{v'T'}$ are the "eddy" correlations of velocity and temperature, and κ_V is the vertical diffusivity. The budget is evaluated with monthly terms, integrated down to depth z_o (250 m), and averaged to produce annual means. The terms in equation (1) represent, from left to right, heat storage, air-sea heat flux, heat advection, Ekman pumping, "eddy" heat flux divergence, and vertical mixing. As in *Colbo and Weller* [2007], we have insufficient observations to calculate the correlations in the eddy heat flux divergence term directly, so this term will be the residual of the budget. We express all of the terms in equivalent heat flux units, W m^{-2}. The terms in equation (1) have units °C s^{-1}; multiplying by $c_p\rho_o$ converts the units to W m^{-2}. A positive heat flux represents warming. For each term in the budget, we calculate the mean annual values as well as the interannual standard error of the mean annual values. The standard error for each term is calculated as $\sigma/\sqrt{n}$, where σ is the standard deviation of the mean annual values and n is the number of years, 6.

We evaluate the heat budget equation using data from the Stratus mooring, which has been deployed at 85°W 20°S in the SEP since November 2000 (Figure 1). The mooring was serviced every year and redeployed in the same location. Complete descriptions of the mooring instruments and their calibration, as well as the standard mooring setup and deployment procedures can be found in *Colbo and Weller* [2007, 2009].

The upper 250 m of the mooring line was heavily instrumented, measuring temperature, salinity, and velocity at 15–20 depth levels (Figure 2a). The vertical positions of the instruments mounted on the mooring line varied slightly between the different deployments. Temperature instruments, primarily SeaBird Electronics SBE-16s, SBE-37s, and SBE-39s, were closely spaced near the surface and more widely spaced at depth. The temperature record (Figure 2b) was interpolated between the surface and 250 m at 5 m spacing. Before computing the heat budget the temperature record was averaged into monthly bins.

The mooring was instrumented with four different types of current meters providing hourly estimates of velocity. An RDI 300 kHz Acoustic Doppler Current Profiler (ADCP) provided velocities near the surface. Point measurement current meters, including Vector Measuring Current Meters, and subsequently Aanderaa and Nortek instruments, were deployed at multiple locations on the mooring line. The velocity record (Figures 2c and 2d) required considerable postprocessing. We examined the current meter records for each mooring deployment and eliminated instruments and ADCP bins that consistently deviated from the other velocity measurements. For example, the ADCP bins shallower than 50 m suffered from low backscatter during the day due to the diel migration of zooplankton, so our analysis retained only bins deeper than 50 m. Using nearest-neighbor interpolation, the uppermost velocity observations from the other current meters (usually

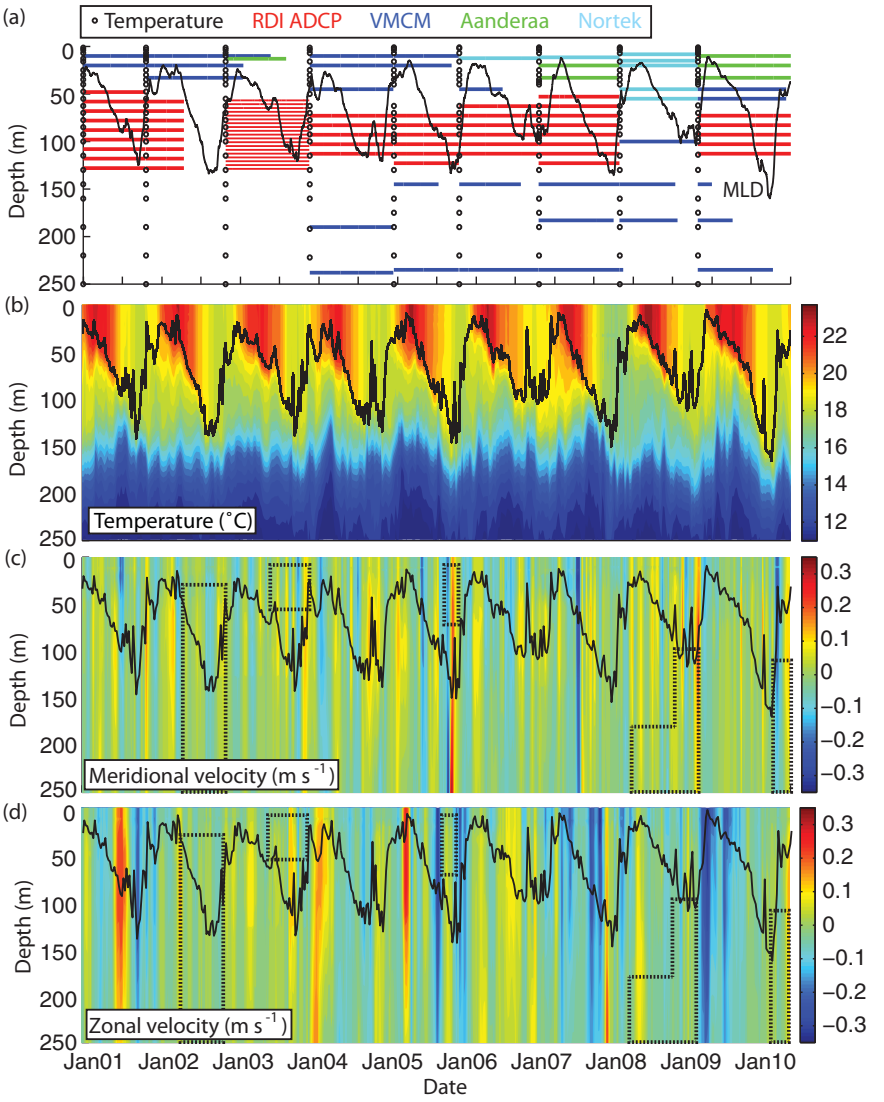

Figure 2. Time series of (a) instrumentation, (b) temperature, (c) meridional velocity, and (d) zonal velocity, averaged into weekly bins, for the first nine Stratus mooring deployments. The mixed layer depth (black line) is plotted in each plot. In Figure 2a, the colored lines represent the depths and measurement durations of the four different types of current meters; the black open circles denote the depths of temperature instrumentation for each deployment. The missing velocity data (dashed boxes in Figures 2c and 2d) were filled as described in section 2.

at around 10 m) were extended to the surface. The current meter records used in the heat budget calculation are shown in Figure 2a.

Some Stratus mooring deployments are missing large sections of velocity data, such as when the ADCP failed during 2002. These periods are denoted by dashed boxes in Figures 2c and 2d. To fill in the missing velocity data, we first create a set of typical velocity profiles by binning the weekly averaged velocity profiles according to their average velocity over the 75–125 m depth range. The 75–125 m depth range tends to have the highest velocities outside of the near-surface layer. The bins are spaced from -0.4 to 0.4 m s^{-1} with a width 0.05 m s^{-1}. For each incomplete weekly averaged velocity profile, the typical profile that most closely matches the incomplete profile's available data in a least squares sense (the typical profile that minimizes the sum of the squared differences between the available data and the typical profile) is then used to fill in the missing velocity data. To compute the heat budget the velocity is averaged into monthly bins and interpolated to the same grid as the temperature measurements.

The surface buoy had redundant systems that measured air and sea surface temperatures, humidity, barometric pressure, wind speed and direction, incoming shortwave and longwave radiation, and precipitation

Table 1. Annual Air-Sea Heat Flux Components (Mean ± Standard Error in Units of W m^{-2})

Period	Net Flux	Shortwave	Longwave	Latent	Sensible
2001–2004	44 ± 5	193 ± 4	−41 ± 1	−99 ± 2	−8 ± 1
2004–2009	32 ± 4	190 ± 2	−44 ± 1	−107 ± 3	−8 ± 1

every minute. *Fairall et al.*'s [2003] COARE 3.0 algorithm was used to calculate the latent and sensible heat fluxes. Further discussion of the annual, interannual, and long-term variability in the surface meteorology and air-sea fluxes at the site is provided by *Weller* [2014].

Our study also employs 12,628 Argo profiles collected between 13 February 2003 and 1 June 2013 in a region extending from 10°S to 30°S and 70°W to 100°W (Figure 1a). Argo floats generally sample to a depth of 2000 m and measure temperature, salinity, and pressure at roughly 75 depth levels. Vertical sample spacing for most floats is less than 20 m to depths of 400 m, below which the spacing increases to 50 m. Argo data are available online at http://www.usgodae.org/argo/argo.html.

A number of satellite products are used in this study. To calculate Ekman pumping and transport, we use surface wind stress fields from the Cross-Calibrated, Multi-Platform (CCMP) Project [*Atlas et al.*, 2011]. The product provides estimates of wind stress on a 0.25° grid at 5 day intervals and is available online at http://podaac.jpl.nasa.gov/. We also use Remote Sensing Systems' optimally interpolated SST fields, produced by blending fields from the TMI and AMSR-E instruments. The product is adjusted to approximate nighttime SSTs with an empirical model of diurnal warming [*Gentemann et al.*, 2003], and is available on a daily, 0.25° grid. This SST product is available online at http://www.ssmi.com/. Merged "Reference" Sea Level Anomaly (SLA) fields from Archiving, Validation, and Interpretation of Satellite Oceanographic (AVISO), available on a weekly, 0.25° grid, and CNES-CLS09 v1.1 mean dynamic topography fields [*Rio et al.*, 2011] are also used to examine changes in circulation near the mooring site. The altimetry data are provided online at http://www.aviso.oceanobs.com. The Multivariate ENSO (El Niño-Southern Oscillation) Index was obtained at http://www.esrl.noaa.gov/psd/enso/mei/index.html.

3. Stratus Mooring Heat Budget

In this section, we examine the terms of the heat budget (equation (1)). Again, a positive heat flux represents warming. For each term, we calculate the 6 year mean value as well as the standard error. The error estimates taken from *Colbo and Weller* [2007] are their estimates of each term's error.

3.1. Heat Storage

On annual time scales, we expect the heat storage term to be approximately zero. Averaged over the 6 year study period, the annual heat storage is 0 ± 0.1 W m^{-2} (mean ± standard error). Some interannual variability is evident in the temperature record (Figure 2b); in particular, the winter of 2006 featured a particularly warm and shallow mixed layer, whereas the winter of 2007 featured an especially cold mixed layer. The mixed layer properties during our study period are similar to those during *Colbo and Weller*'s [2007] study period; the average mixed layer was only 0.1°C warmer and 0.5 m deeper during our study period.

3.2. Air-Sea Heat Flux

The net heat flux over our study period is 32 ± 4 W m^{-2} (Table 1 and Figure 3). This flux is considerably smaller than the net heat flux of 44 ± 5 W m^{-2} observed by *Colbo and Weller* [2007]. The decreased net heat flux is mostly due to an increase in ocean latent heat loss, although a reduction in incoming shortwave radiation and an increase in ocean long wave cooling also contributes (Table 1). Compared to the average annual cycle over 2001–2004, the typical year from 2004 to 2009 features a longer period of ocean heat loss during the winter, as well as a consistently weaker net heat flux throughout the entire year (Figure 4b). Precipitation at the Stratus mooring is minimal and the latent heat flux is relatively strong (Figures 3a and 3c), corresponding to an annual evaporation rate of nearly 1.3 m of freshwater per year.

The mooring is located south of the center of the trade wind jet, and so the mooring mostly measures the southeasterly trade winds (Figure 3b). The average wind stress over 2004–2009 increased 15% relative to 2001–2004 (Figures 3b and 4c). Besides strengthening, the winds shifted 3° westward for 2004–2009 relative to 2001–2004. This increase in wind stress likely influenced the observed changes in the air-sea fluxes,

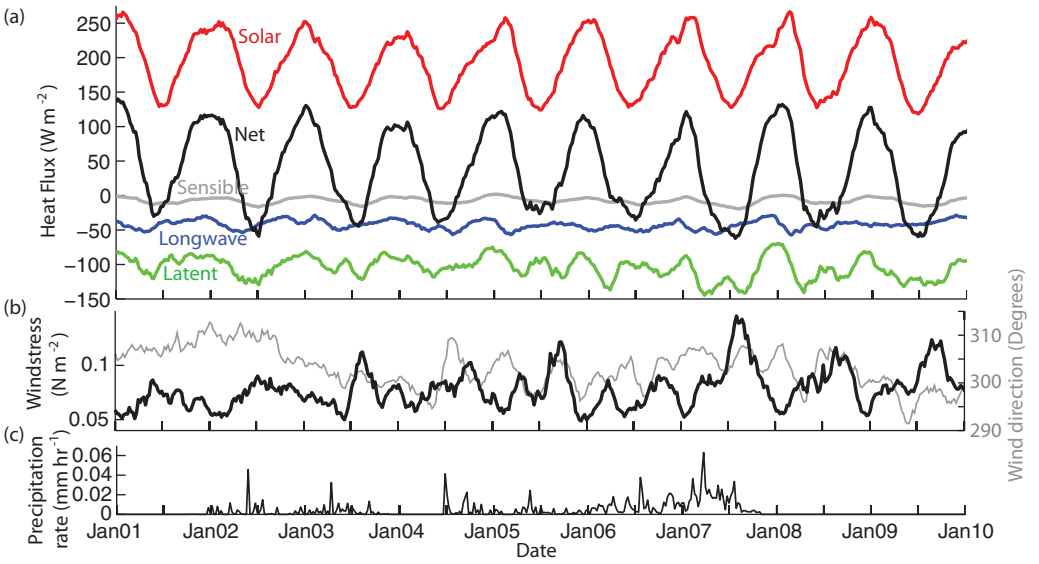

Figure 3. Weekly averaged (a) air-sea heat flux components, (b) wind stress (black line) and wind direction (gray line), and (c) precipitation. The mooring measures solar (red line) and longwave (blue line) fluxes, whereas the latent (green line) and sensible (gray line) fluxes are estimated using the COARE 3.0 algorithm [*Fairall et al*., 2003]. The fluxes and winds are smoothed with a 2 month running mean.

as well as the changes in Ekman transport and pumping. The winds exhibit a consistent annual cycle, particularly during 2004–2009; winds are weakest from December to February and gradually increase to a maximum in September (Figure 4c). Further discussion of the air-sea fluxes at the Stratus mooring are provided by *Weller* [2014], who identified long-term trends in wind stress, latent heat flux, and net heat flux.

3.3. Advection

We employ a new method for estimating the advection term of the heat budget. We make monthly estimates of heat advection at the mooring using profiles of the horizontal temperature gradient calculated with Argo data. Our advection term includes contributions from the gyre circulation, Ekman transport, and eddies. To calculate the temperature gradient, we utilize the 15 Argo profiles closest to the mooring for each month; as an illustration, the 15 profiles closest to the Stratus mooring from March 2008 are shown in Figure 1a. The average distance between the 15 profiles and the mooring is fairly uniform, approximately 300 km; the mean meridional distance is slightly smaller than the mean zonal distance. The profile of the horizontal temperature gradient for each month is found by fitting best fit planes at 5 m intervals from the surface to 250 m to the Argo temperature and salinity profiles.

By evaluating the plane fits at the Stratus mooring's location and averaging over the mixed layer, we create an estimate of the time series of mixed layer temperature at the mooring (Figure 5). For much of the record, the Argo-derived mixed layer temperature estimate closely matches the observed monthly mixed layer temperature at the mooring. The average root-mean-square difference between the two records is 0.29°C, with the largest differences occurring in March, April, and May (particularly for 2009), when the SSTs are warmest and the mixed layer depth is shallowest (Figures 4a and 4d). The similarity between the observed and estimated mixed layer temperature records gives us confidence that our method for estimating the horizontal temperature gradient is effective.

The mean horizontal temperature and salinity gradients at the Stratus mooring reflect the hydrographic features of the SEP (Figure 6). The mean zonal temperature gradient at the mooring is negative from the surface to 250 m depth (Figure 6c). Coastal upwelling, driven by northward winds along South America, causes isopycnals to tilt up toward the coast, bringing cooler subsurface waters closer to the surface [*Blanco et al*., 2001; *Schneider et al*., 2003]. Evaporation greatly exceeds precipitation in the center of the SEP's subtropical gyre, creating a warm and salty surface layer known as Subtropical Surface Water to the west. Eastern South Pacific Intermediate Water, identifiable as a shallow salinity minimum layer that originates in the eastern South Pacific, exists below the surface layer and shoals and freshens toward shore and to the north [*Reid*,

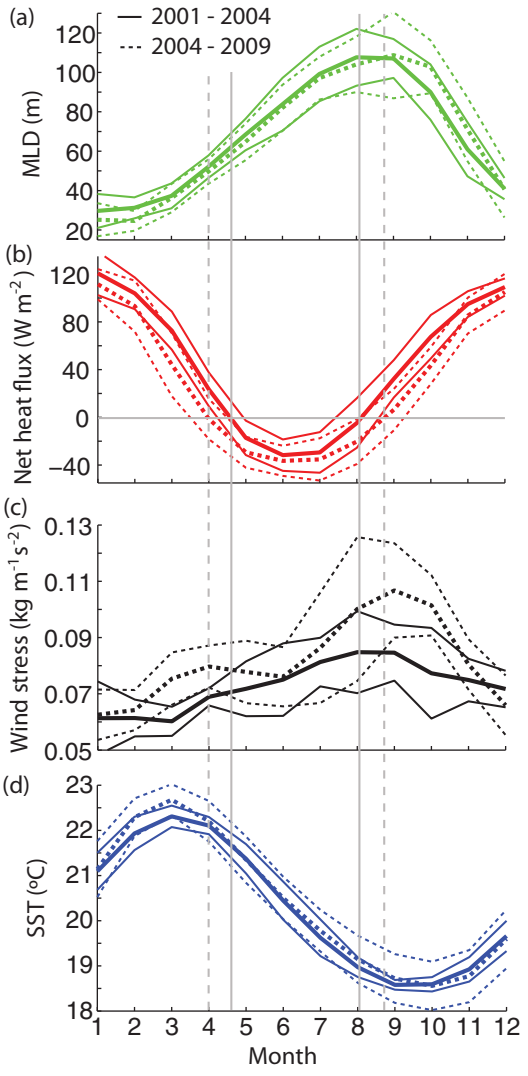

Figure 4. Average annual cycles of (a) mixed layer depth (MLD), (b) net heat flux, (c) wind stress, and (d) SST at the Stratus mooring for two time periods, 2001–2004 (solid lines) and 2004–2009 (bold dashed lines). For each time period, the daily values of the variables were first smoothed with a 45 day running average and then binned by month. The standard deviation is shown for the 2004–2009 period (thin dashed lines). The vertical gray lines denote the zero crossings of the net heat flux for the two time periods.

1973; *Tsuchiya and Talley*, 1998; *Schneider et al*., 2003; *Karstensen*, 2004]. The zonal salinity gradient changes sign below the salinity minimum layer (Figure 6g).

The mean meridional temperature gradient at the Stratus mooring is more complicated; it is negative from approximately 75 to 200 m depth (cooler water toward the north), and is mostly smaller than the zonal gradient at the mooring (Figure 6d). The Stratus mooring corresponds to approximately the deepest point in the "trough" structure of the gyre, visible in the mixed layer and temperature structure in Figure 6b; this "trough" structure causes the meridional temperature gradient to change sign. If the mooring was located at 22°S, the meridional temperature gradient would be positive to a depth of approximately 150 m, and much more similar to the meridional temperature gradient used in *Colbo and Weller* [2007, Figure 10], which was positive to a depth of 200 m. The mean meridional salinity gradient is positive at all depths (Figure 6h).

The mean flow measured at the Stratus mooring is weak. It features southwestward Ekman transport at the surface and northwestward gyre-scale mean flow at depth (Figures 1b, 7b, and 7c). Over 2004–2009, the mean zonal velocity was negative (offshore) at all depths; this contrasts with the mean zonal velocity over 2001–2004, which was smaller and onshore over 50–250 m depth (Figure 7b). *Colbo and Weller* [2007] noted that the velocity during their study period was predominately northward, as zonal flows were particularly weak during their study. This was unexpected, as previous studies had found evidence for more zonal flows [*Johnson and McPhaden*, 1999], similar to the mooring observations over 2004–2009.

The velocity record at the mooring is highly variable (Figures 2c and 2d). Strong velocity pulses, likely due to eddies, are much larger than the mean velocity (Figure 7a). Eddies in the SEP have propagation speeds on the order of 3 cm s^{-1} [*Chaigneau and Pizarro*, 2005a] and the average eddy radius in the SEP is approximately 85 km [*Chelton et al*., 2011; *Holte et al*., 2013]. This suggests that it takes the average eddy more than 2 months to transit past the mooring. Therefore, as most eddies in the SEP have time scales greater than a month, some eddy signals are expected to be captured in our calculation. Averaging the budget over annual and longer time scales smooths the eddy signals, which are evident as large variations in the advective heat flux.

Integrated from 0 to 250 m, the mean advective heat flux at the Stratus mooring is -41 ± 29 W m^{-2}, with a cooling zonal component and a warming meridional component (Figure 8). Again, this heat advection is due to a combination of geostrophic gyre circulation, Ekman transport, and eddy contributions. The large

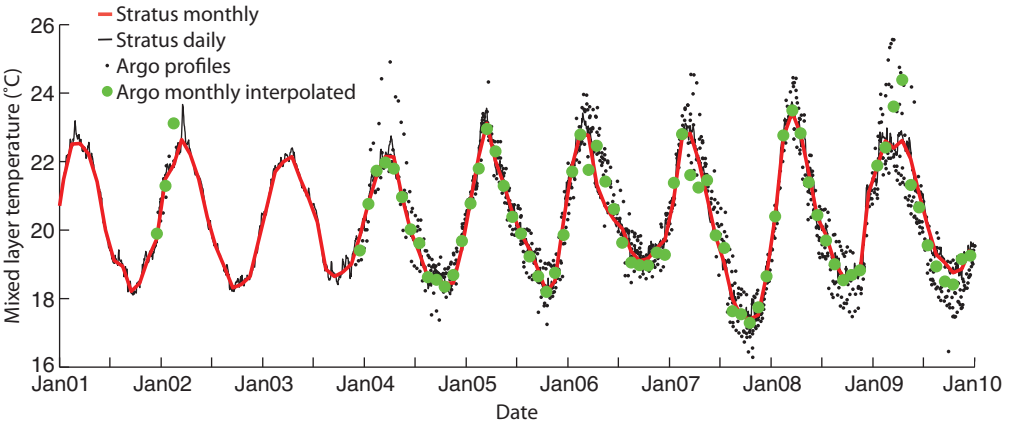

Figure 5. Time series of the Stratus mooring's monthly (red line) and daily (black line) mixed layer temperatures. For each month, the mixed layer temperatures of the 15 Argo profiles closest to the mooring are also plotted (black dots). The monthly planes fits to the Argo mixed layer temperatures, evaluated at the Stratus mooring's location, are also plotted (green dots).

cool advection in the surface layer is likely due to Ekman transport. Much like the velocity record, the time series of the monthly advective heat flux is dominated by large pulses likely associated with eddies; this variability is reflected in the relatively large standard error. The strongest advective cooling occurred in 2007, during a La Niña year, due to particularly strong offshore zonal velocities.

Our estimate of the advective heat flux contrasts with *Colbo and Weller* [2007], who calculated a flux of -14 ± 5 W m^{-2}, due primarily to cool geostrophic advection in the meridional direction and to a warming Ekman transport. To calculate the component of the advective heat flux due to geostrophic circulation, *Colbo and Weller* [2007] used a World Ocean Atlas historical climatology to estimate the meridional temperature gradient; they used a collection of CTD and XBT profiles to estimate the zonal temperature gradient, as the atlas had a resolution of 10° longitude by 1° latitude. Both gradient estimates were fixed in time. The mean geostrophic velocity profile was computed by temporally averaging the velocity record beneath 58 m. *Colbo and Weller* [2007] computed a geostrophic heat advection of -20 W m^{-2}, mostly due to meridional heat advection. To estimate the advective heat flux due to Ekman transport, *Colbo and Weller* [2007] used weekly averaged satellite wind and SST fields; they found a warming Ekman heat flux of 6 W m^{-2}. Our advective heat flux, as well as the differences in the advective heat flux between our study and *Colbo and Weller* [2007] are further discussed in section 5.

3.4. Ekman Pumping

To estimate the Ekman pumping term, we follow the same procedure as *Colbo and Weller* [2007] and obtain the vertical velocity profile by assuming Sverdrup dynamics. Using Argo and QuikSCAT data, *Gray and Riser* [2014] found that over the subtropics and tropics, including the SEP, Sverdrup balance provided a reasonable quantitative picture of the observed circulation. We assume that beneath the Ekman layer the eddy signal averages out over the 6 years of our study. We apply the Sverdrup relation, $w_z = \beta v/f$, to the monthly meridional velocities, obtaining monthly profiles of the gradient of the vertical velocity. The w_z profile is integrated downward from a depth of 20 m such that the near surface maximum in the vertical velocity matches the Ekman pumping velocity derived from CCMP wind fields, providing a profile of the vertical velocity at the mooring. Ideally, we would integrate Sverdrup balance from the surface, where the vertical velocity must be zero, to avoid uncertainties associated with matching the near surface velocity maximum to the Ekman pumping velocity. However, as noted by *Colbo and Weller* [2007], the mooring does not resolve the velocity in the upper 20 m well enough to integrate from the surface. Profiles of the annual displacement are shown in Figure 9a.

The Ekman pumping term contributes 10 ± 9 W m^{-2} to the heat budget (Figure 9b). This is larger than the 3 ± 5 W m^{-2} found by *Colbo and Weller* [2007]. This is likely due to slight differences in the meridional velocity over the two time periods (Figure 7c). In particular, the mean meridional velocity for 2006 was negative at all depths, contrasting with all of the other annual means. Excluding this year reduces our estimate of the Ekman pumping term to 6 W m^{-2}, which is much closer to the Ekman pumping term in *Colbo and*

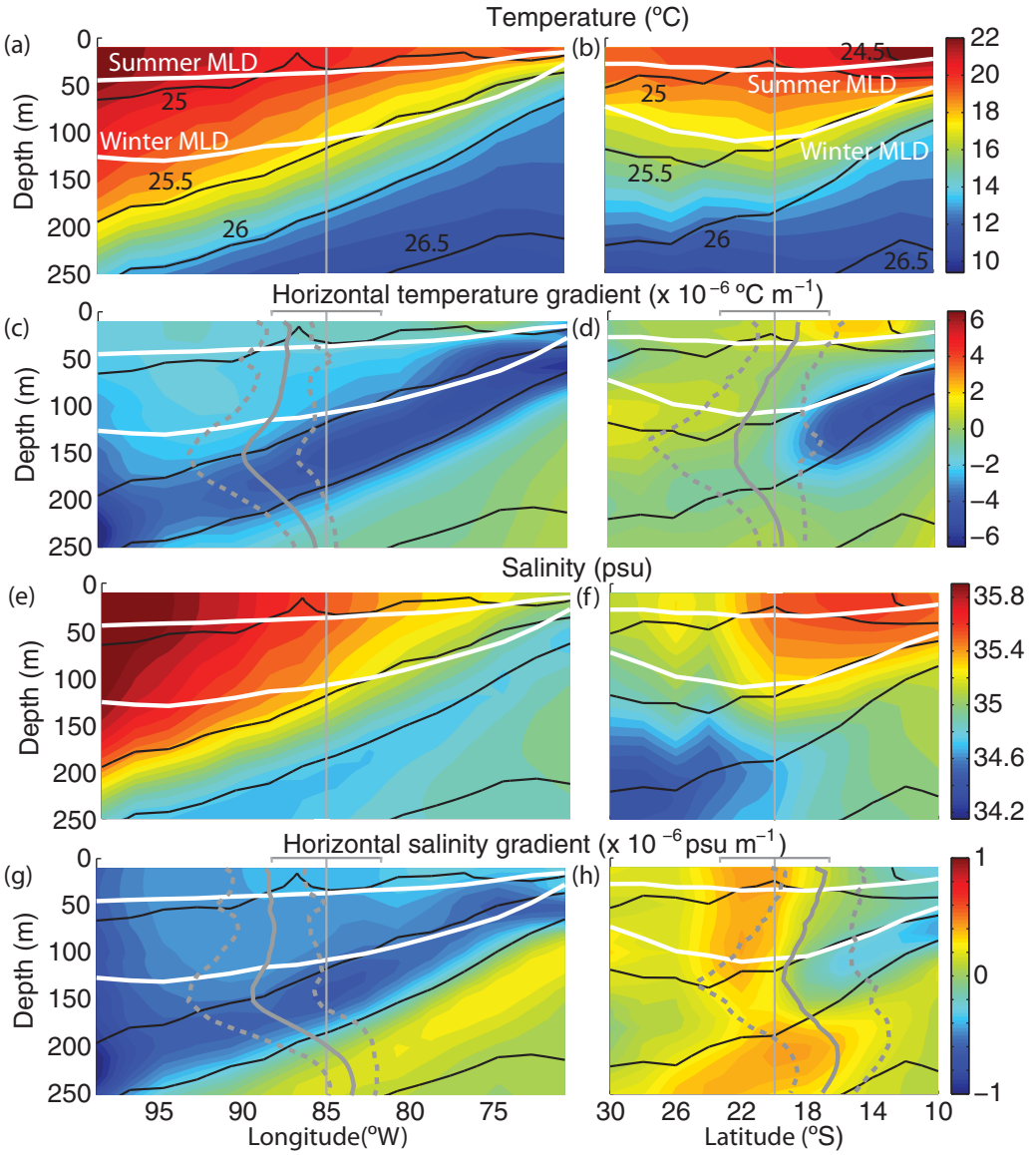

Figure 6. (left column) Composite Argo zonal and (right column) meridional sections of (a and b) temperature, (c and d) temperature gradient, (e and f) salinity, and (g and h) salinity gradient. The zonal and meridional sections were computed along 20°S and 85°W, respectively, by averaging Argo profiles in 2° (along-section) by 6° (cross section) bins. Potential density (black lines) is contoured along the 25.0, 25.5, 26.0, and 26.5 kg m^{-3} isopycnals. The summer and winter MLDs are marked by white lines. The thin vertical gray lines denote the location of the Stratus mooring, as well as zero crossings for the means of the monthly gradient estimates at the mooring (bold gray lines) and their standard deviations (dashed gray lines); the scale denotes gradients of $\pm 4 \times 10^{-6}$°C m^{-1} and $\pm 0.4 \times 10^{-6}$ psu m^{-1}.

Weller [2007]. The CCMP wind fields also indicate that the Ekman pumping velocity at the base of the Ekman layer increased by approximately 1 m yr^{-1} for 2004–2009 relative to 2001–2004.

3.5. Vertical Mixing

The Stratus mooring's temperature record features a small vertical temperature gradient at 250 m, approximately 0.02°C m^{-1} (Figure 2b). As in *Colbo and Weller* [2007], we assume a vertical diffusivity (κ_v) of 3×10^{-5} m^2 s^{-1}, leading to an average annual heat flux of -3 ± 0.1 W m^{-2} due to vertical mixing. This matches the mean value calculated by *Colbo and Weller* [2007].

3.6. Residual

The terms of the Stratus mooring heat budget are shown in Table 2, both for our 2004–2009 budget and for *Colbo and Weller*'s [2007] 2001–2004 budget. There are considerable differences in the budgets,

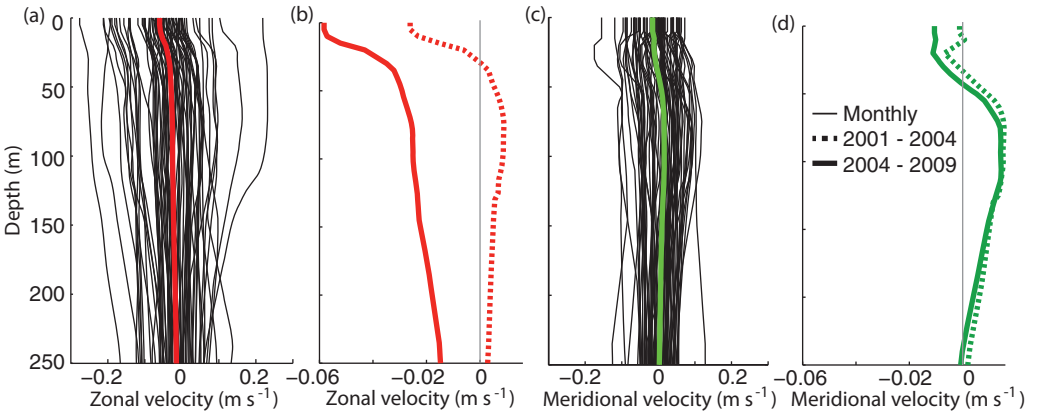

Figure 7. Stratus mooring velocity averaged into (a) monthly zonal velocity profiles (thin black lines), (b) mean zonal velocity, (c) monthly meridional velocity profiles (thin black lines), and (d) mean meridional velocity. In Figures 7a and 7c, the mean zonal and meridional velocities averaged over 2004–2009 are plotted (red and green lines, respectively). In Figures 7b and 7d, the mean zonal and meridional velocities are averaged over two time periods, 2001–2004 (dashed lines) and 2004–2009 (solid lines).

particularly for the advective heat flux and for the net air-sea heat flux, as well as for the residual. We estimated a much larger advective cooling term at the mooring than *Colbo and Weller* [2007]. Similarly, over 2004–2009, the mooring observed a smaller air-sea heat flux than for *Colbo and Weller*'s [2007] study period, 2001–2004. The residual of our budget is 2 ± 29 W m^{-2}, whereas *Colbo and Weller*'s [2007] budget has a residual of -30 ± 12 W m^{-2}. The differences between the two budgets, as well as their interpretation, are discussed in section 5.

4. Salinity Budget

We also calculate a salinity budget for 2004–2009 using Stratus mooring and Argo data. The salinity budget has the same formulation as the heat budget, although the air-sea flux term takes the form $(E-P)S$. Salinity (S) and precipitation (P) are measured. Evaporation (E) is calculated using $E = Q_{LH}/\rho l_e$, where Q_{LH} is the latent heat and l_e is the latent heat of vaporization. Integrating the salinity budget over the year gives salinity flux in units of psu m. A negative term implies freshening, whereas a positive term implies salinification.

As with the heat budget, our salinity budget suggests that mean advection (-60 ± 34 psu m) largely compensates for the substantial amount of freshwater removed by evaporation in the SEP ($E-P$ of 47 ± 1.3 psu m) (Table 3). As with the heat budget, the salinity advection term is highly variable. The residual of our salinity budget is small, -2 ± 34 psu m. The air-sea flux term is larger for 2004–2009 than for *Colbo and Weller*'s [2007] budget because the latent heat flux increased by 8 W m^{-2} compared to 2001–2004 (Table 1). In general our salinity budget is fairly similar to *Colbo and Weller*'s [2007] salinity budget.

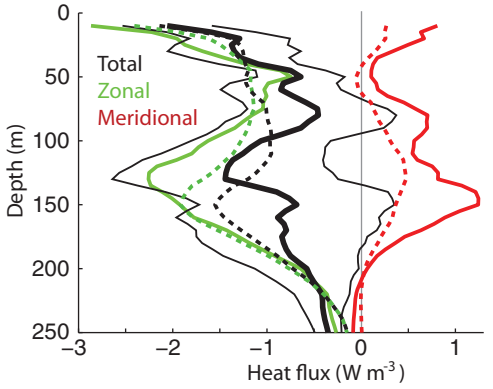

Figure 8. Vertical profiles of the mean heat advection over 2004–2009: total heat advection (solid black line), zonal heat advection (solid green line), and meridional heat advection (solid red line). The thin black lines represent the standard error of the total heat advection. The dashed lines represent the products of the mean temperature gradient profiles and the mean velocity profiles.

5. Discussion and Summary

The southeast Pacific Ocean (SEP) features one of the world's largest subtropical stratocumulus cloud decks, making it important to global climate. The clouds are maintained over the SEP's relatively cool SST, so changes in the upper ocean heat content of the SEP could affect the global climate system's absorption of solar radiation, as well as the substantial fisheries in the upwelling region off of the coasts of Chile and Peru. These clouds and their radiative effects

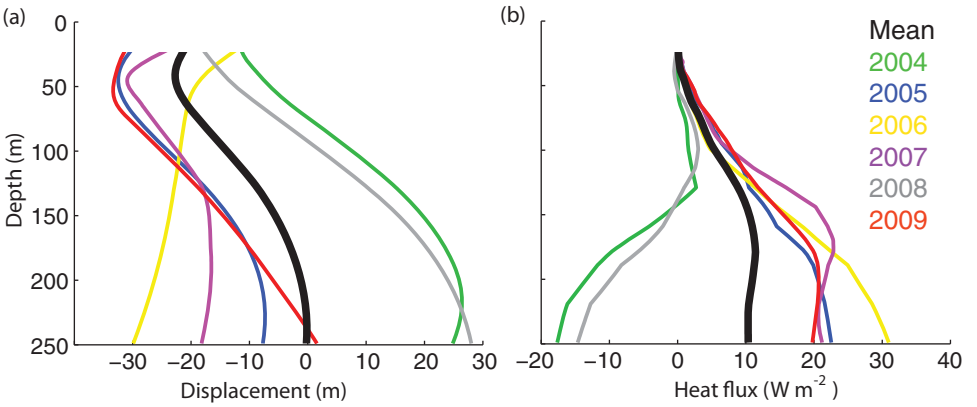

Figure 9. Profiles of (a) vertical displacement over a year due to Ekman pumping and (b) vertical heat flux integrated from the surface to depth z.

were characterized in *de Szoeke et al.* [2012]. Many coupled GCMs struggle to reproduce the extensive stratus clouds or the cool SSTs of the SEP [*Mechoso et al.*, 1995; *Ma et al.*, 1996; *de Szoeke and Xie*, 2008; *Lauer et al.*, 2010]. Improving our understanding of the heat budget of the SEP will allow us to better understand climate variability in this region.

Numerous processes contribute to the SEP's upper ocean heat balance, including gyre circulation, Ekman transport, and pumping, vertical mixing, and horizontal eddy heat flux divergence. The SEP is a region of net ocean heat gain through air-sea fluxes [*Colbo and Weller*, 2007; *Yu and Weller*, 2007]. We assess the annual heat budget of the SEP for the period 2004–2009, using data from the upper 250 m of the Stratus mooring, located at 85°W 20°S, and Argo floats, in order to understand how the SEP maintains relatively cool SSTs despite such strong surface forcing.

Our primary findings are as follows. We find that a cool advective heat flux of -41 ± 29 W m^{-2}, accomplished by a combination of the mean gyre circulation, Ekman transport, and eddies, compensates for a warming air-sea heat flux of 32 ± 4 W m^{-2}; vertical mixing and Ekman pumping terms contribute an additional 7 W m^{-2} of warming. The advection term is highly variable year to year, likely due to the passage of eddies. Compared to *Colbo and Weller*'s [2007] heat budget for the 2001–2004 period, our advective term accomplishes much more cooling (-41 W m^{-2} versus -14 W m^{-2}) and our observed air-sea heat flux is smaller (32 W m^{-2} versus 44 W m^{-2}). The residual of our budget, 2 ± 29 W m^{-2}, is much smaller than the -30 ± 12 W m^{-2} residual of *Colbo and Weller*'s [2007] budget. The differences between the two budgets, examined more thoroughly below, are due to a combination of different observation periods and different methodologies. A salinity budget also confirms that advection of freshwater (-60 psu m), primarily in the zonal direction, replenishes the freshwater lost through evaporation (47 psu m) and to Ekman pumping (14 psu m).

Our method of calculating the advective term of the heat budget differs greatly from the method employed by *Colbo and Weller* [2007]. We use Argo profiles to estimate the horizontal temperature gradients near the Stratus mooring. With the available Argo coverage we can generate monthly estimates of the horizontal temperature gradient profiles; these gradients are combined with the mooring's velocity record to estimate the heat advection. An estimate of the mixed layer temperature at the mooring derived from the monthly Argo gradients (Figure 5) closely matches the observed mooring mixed layer temperatures. Our advection term includes contributions from the mean gyre circulation, Ekman transport, and eddies, whereas *Colbo*

Table 2. Heat Budget Terms (W m^{-2})[a]

	Surface Flux	Advection	Ekman	Ekman Pumping	Vertical Mixing	Residual
Colbo and Weller	44 ± 5	-20 ± 5	6 ± 4	3 ± 5	-3 ± 2	-30 ± 12
2004–2009	32 ± 4	-41 ± 29	NA	10 ± 9	-3 ± 0.1	2 ± 29

[a]*Colbo and Weller*'s [2007] terms include their estimates of the total error; ours include the standard error. *Colbo and Weller* [2007] interpreted the residual as the eddy heat flux divergence.

Table 3. Salinity Budget Terms (psu m)[a]

	Surface Flux	Advection	Ekman	Ekman Pumping	Vertical Mixing	Residual
Colbo and Weller	40 ± 4	-52 ± 3	6 ± 5	16 ± 5	1 ± 1	-11 ± 5
2004–2009	47 ± 1.3	-60 ± 34	NA	14 ± 4	1 ± 0.2	-2 ± 34

[a]*Colbo and Weller*'s [2007] terms include their estimates of the total error; ours include the standard error.

and Weller's [2007] advective term includes contributions from the mean gyre circulation and Ekman transport. *Colbo and Weller* [2007] relied on the World Ocean Atlas historical climatology to estimate the meridional temperature gradient and on a collection of CTD and XBT profiles to estimate the zonal temperature gradient. These gradients were fixed in time. They used satellite fields to estimate the heat advection due to Ekman transport.

Our advective term, -41 ± 29 W m^{-2}, has a much larger cooling influence than the -14 ± 4 W m^{-2} advective term calculated by *Colbo and Weller* [2007] (Table 2). Our cooling was primarily due to zonal advection (Figure 8), whereas for *Colbo and Weller* [2007] it was primarily due to meridional advection. It is difficult to directly compare the advection estimates because the methods and data used in computing them are so different. An analysis of heat advection by mean fields using 2009 World Ocean Atlas data [*Locarnini et al*., 2010] to calculate the temperature gradients reveals that the difference in heat advection between our budget and *Colbo and Weller* [2007] was primarily due to changes in the zonal velocity. Changes in the meridional temperature gradient and Ekman transport also contributed to the difference in heat advection.

Over 2001–2004, the meridional velocity and zonal velocities at the Stratus mooring had similar magnitudes, whereas our study period featured stronger offshore zonal flows (Figure 7) more in line with previous studies, such as *Johnson and McPhaden* [1999]. This increase in the offshore zonal flow was also observed in geostrophic velocities calculated using AVISO SLA and CNES-CLS09 v1.1 mean dynamic topography fields [*Rio et al*., 2011] and an assumption of geostrophic balance. The mean dynamic topography for 2004–2009 is shown in Figure 1b; the geostrophic velocities follow the mean dynamic height contours. The AVISO-derived offshore zonal geostrophic velocity at the mooring increased by approximately 2 cm s^{-1} during our study period compared to 2001–2004.

Our mean meridional temperature gradient differs from *Colbo and Weller*'s [2007] mean meridional temperature gradient. Our temperature gradient is negative from 75 to 200 m (Figure 6d), producing warm meridional advection (Figure 8). In the World Ocean Atlas data used by *Colbo and Weller* [2007], however, the meridional temperature gradient at the Stratus mooring was positive to a depth of 200 m, producing cool meridional advection. This discrepancy is likely tied to the mooring's position in the "trough" structure of the gyre, close to a region where meridional gradients change sign (Figures 6b and 6d). *Colbo and Weller* [2007] noted that uncertainties in the World Ocean Atlas fields were likely to be the largest source of error in their advection calculation. Based on the differences in the meridional gradient, it seems likely that the center of the Atlas gyre's "trough" is shifted northward relative to the "trough" in the Argo observations.

Colbo and Weller [2007] calculated a warm Ekman transport of 6 ± 4 W m^{-2}, whereas we identified a cool Ekman transport (Figure 8). The warm Ekman advection surprised *Colbo and Weller* [2007], as they had anticipated that Ekman transport would transport cool coastal waters offshore. In a modeling study, *Colas et al*. [2011] found a cooling Ekman transport in the SEP, in line with our results. Recalculating *Colbo and Weller*'s [2007] satellite-based Ekman transport with CCMP winds and new SST fields, we find a cool Ekman transport for their study period, as well as ours, of approximately -2 W m^{-2}. The seasonal cycle likely affects Ekman transport because the largest zonal SST gradients (most negative) occur in August, September, and October, when the winds are strongest. The enhanced cooling due to Ekman transport for our budget could also be tied to the increase in winter wind stress for 2004–2009 (Figure 4c).

The net air-sea heat flux during our study period, 32 ± 4 W m^{-2}, is approximately two-thirds of the flux observed during *Colbo and Weller*'s [2007] study period, 44 ± 5 W m^{-2} (Table 1 and Figure 4). *Weller* [2014] thoroughly documented the trends in the Stratus moorings' air-sea flux observations, including a decrease in the net air-sea heat flux of approximately 4 W m^{-2} per year. It is uncertain how this reduction in the air-sea heat flux will impact the local heat and salt balances, as less net warming may reduce the stability of the upper ocean and enhance vertical mixing.

The residual of our budget, 2 ± 29 W m^{-2}, is much smaller than the -30 ± 12 W m^{-2} residual of *Colbo and Weller*'s [2007] budget. *Colbo and Weller* [2007] interpreted their budget's residual as the eddy heat flux divergence; they reasoned that eddies in the SEP, which form near the coast, transport cool, coastal water offshore, thus providing the necessary cooling at the mooring. Recent studies, however, have suggested that eddies are likely not crucial to the upper ocean heat budget of the SEP [*Zheng et al*., 2010; *Toniazzo et al*., 2010; *Colas et al*., 2011; *Holte et al*., 2013]. Some eddy signal is incorporated into our mean monthly heat advection term; by computing the heat advection due to mean fields (dashed lines in Figure 8) and comparing it to the mean monthly heat advection, we can isolate a portion of the eddy signal. The heat advection by mean fields is slightly greater, -49 W m^{-2}, suggesting that processes on shorter time scales (potentially eddies) have a warming influence at the Stratus mooring. Similarly, the salinity advection by mean fields is -69 psu m, suggesting that processes on shorter time scales increase the salinity at the mooring, counter to the mean advective freshening. Anticyclonic eddies in the SEP are associated with warm and saline anomalies [*Chaigneau and Pizarro*, 2005a; *Holte et al*., 2013]. Using the *Chelton et al*. [2011] eddy census, we find that seven more anticyclonic eddies passed within 3° of the mooring than cyclonic eddies over 2004–2009, potentially accounting for the difference between the mean heat advection and the heat advection by mean fields. But to put this in perspective, this should be considered a mere sampling artifact. The eddies are too variable and there are too few of them to identify their rectified effect with any certainty.

Some of the differences between *Colbo and Weller*'s [2007] 2001–2004 budget and our 2004–2009 budget could be due to the interannual variability of the SEP. The Multivariate ENSO Index, mostly positive from 2001 to 2006, was strongly negative during the 2007–2008 La Niña. The water column at the Stratus mooring was particularly cool and fresh in 2007 and 2008; the especially cold mixed layers during the winter of 2007 are evident in Figures 2b and 5. The strongest cool/fresh advection occurred in 2007, primarily due to enhanced zonal advection. The winter of 2006 featured a particularly warm and shallow mixed layer (Figure 2b), the strongest warm/salty advection, primarily zonal, and the largest Ekman pumping heat flux (Figure 9b). This correspondence suggests a connection between advection and the interannual variability of the upper ocean temperature at the mooring location. Similarly, in a modeling study, *Shinoda and Lin* [2009] found that heat advection associated with ENSO events primarily controlled the interannual SST variation in the stratus cloud region north of 20°S, although they found that meridional advection was more important than zonal advection. The positive ENSO index during 2001–2004 suggests that *Colbo and Weller*'s [2007] budget may have been calculated for a period of reduced advective cooling.

The homogeneity of many meteorological and oceanographic observations of the SEP leads us to speculate that similar air-sea forcing, dynamics, and heat balances likely predominate over a wide swath of the SEP near the Stratus mooring. From the perspective of the surface forcing, the SEP is characterized by a lack of synoptic weather systems, as their passage is blocked to the east by the Andes, and surface forcing fields, in general, have the spatial scale of the South Pacific high-pressure cell. *de Szoeke et al*. [2012] examining the air-sea fluxes along 20°S, 75°W–85°W from a number of cruises to the Stratus mooring, noted that despite zonal gradients in boundary layer and cloud vertical structure, surface radiation and cloud radiative forcing were relatively uniform in longitude. No permanent frontal structures have been observed along 20°S, 75°W–85°W in hydrographic data collected on cruises to the mooring. Similarly, the Argo composite zonal temperature gradient exhibits a consistent pattern (Figure 6). If zonal flows are directed offshore, as is suggested in Figure 1, then we can expect zonal advective cooling throughout this longitude range. Zonal advection is the dominant cooling term for the Stratus mooring heat budget. The meridional temperature gradient changes sign to the north of the mooring, so it is difficult to extrapolate meridional heat advection beyond the Stratus mooring. Consistent with the small residual (eddy heat flux divergence) of our budget, *Chaigneau and Pizarro* [2005b] observed weak eddy kinetic energy offshore in the SEP, including near the Stratus mooring. While these observations suggest that, in general, the dominant terms of our budget could hold over a considerable region near the Stratus mooring, there are not enough observations, particularly of velocity, to verify this conjecture.

Although GCM results might not be representative of individual points, our results are supported by a number of recent modeling studies. *Zheng et al*. [2010] found that the net incoming solar heat flux of 18 W m^{-2} was nearly fully balanced by the gyre circulation of upwelled cold water from the coast. *Colas et al*. [2011] found that a combination of mean circulation, with a small contribution from Ekman transport, balanced

atmospheric heating of approximately 20 W m^{-2}. *Toniazzo et al*. [2010] noted the importance of transient features to the SEP's heat budget, as well as the necessity of taking long-term averages. These modeling studies also argued that the eddy heat flux divergence was not spatially coherent, and therefore was unlikely to contribute to the SEP's heat balance as suggested by *Colbo and Weller* [2007].

Our results suggest that in order for GCMs to correctly model the SEP, they must accurately reproduce horizontal temperature and salinity gradients and velocities. Similarly, *Colas et al*. [2011] noted that in many GCMs a misrepresentation of the upwelling circulation, the Peru-Chile Undercurrent, and mesoscale eddies changed the offshore gradients and velocities. *Zheng et al*. [2011] examined 19 coupled GCMs and found that biases in heat transport by Ekman currents largely contributed to the warm SST biases both near the coast and in the open ocean. Improving GCM representations of the SEP will better allow us to understand model projections of climate change.

The large standard error in the advection term (Figure 8) suggests that continued observations from the Stratus mooring are crucial. Assessing the heat budget on shorter time scales is difficult because of the large eddy signals, particularly in velocity (Figure 7a); the temperature gradients do not vary as greatly as the velocity. Our individual annual budgets vary considerably, and only by averaging over 6 years does the residual shrink. It is unknown how climate change will influence the SEP, perhaps leading to decreased trade winds [*Vecchi et al*., 2006] or increased trade winds (R. Weller, submitted manuscript, 2014); there will be continuing challenges in understanding the local heat and salt balances of the upper ocean in such nonstationary conditions.

Acknowledgments
This work was supported by NOAA's Climate Program Office and by NSF grant OCE-0745508. Microwave OI SST data are produced by Remote Sensing Systems and sponsored by National Oceanographic Partnership Program (NOPP), the NASA Earth Science Physical Oceanography Program, and the NASA MEaSUREs DISCOVER Project. They are available online at http://www.ssmi.com/. The altimeter SLA fields are produced by Ssalto/Duacs and distributed by AVISO with support from Centre National d'Etudes Spatiales (CNES). MDT_CNES-CLS09 was produced by CLS Space Oceanography Division and distributed by Aviso, with support from CNES. The altimetry data are provided online at http://www.aviso.oceanobs.com. Argo data are available online at http://www.usgodae.org/argo/argo.html. Data from the Stratus mooring are available at http://uop.whoi.edu/projects/stratus/stratusarchive.html. Surface wind stress fields from the Cross-Calibrated, Multi-Platform (CCMP) Project are available online at http://podaac.jpl.nasa.gov/. The Multivariate ENSO (El Niño-Southern Oscillation) Index was obtained at http://www.esrl.noaa.gov/psd/enso/mei/index.html. The comments of three reviewers greatly improved the manuscript.

References

Atlas, R., R. N. Hoffman, J. Ardizzone, S. M. Leidner, J. C. Jusem, D. K. Smith, and D. Gombos (2011), A cross-calibrated, multiplatform ocean surface wind velocity product for meteorological and oceanographic applications, *Bull. Am. Meteorol. Soc.*, *92*, 157–174.

Blanco, J. L., A. C. Thomas, M.-E. Carr, and P. T. Strub (2001), Seasonal climatology of hydrographic conditions in the upwelling region off northern Chile, *J. Geophys. Res.*, *106*, 11,451–11,468.

Boville, B. A., and P. R. Gent (1998), The NCAR climate system model, Version 1, *J. Clim.*, *11*, 1115–1130.

Chaigneau, A., and O. Pizarro (2005a), Eddy characteristics in the eastern South Pacific, *J. Geophys. Res.*, *110*, CO6005, doi:10.1029/2004JC002815.

Chaigneau, A., and O. Pizarro (2005b), Mean surface circulation and mesoscale turbulent flow characteristics in the eastern South Pacific from satellite tracked drifters, *J. Geophys. Res.*, *110*, C05014, doi:10.1029/2004JC002628.

Chaigneau, A., M. Le Texier, G. Eldin, C. Grados, and O. Pizarro (2011), Vertical structure of mesoscale eddies in the eastern South Pacific Ocean: A composite analysis from altimetry and Argo profiling floats, *J. Geophys. Res.*, *116*, C11025, doi:10.1029/2011JC007134.

Chelton, D. B., M. G. Schlax, and R. M. Samelson (2011), Global observations of nonlinear mesoscale eddies, *Prog. Oceanogr.*, *91*, 167–216.

Colas, F., J. McWilliams, X. Capet, and J. Kurian (2011), Heat balance and eddies in the Peru-Chile Current System, *Clim. Dyn.*, *39*(1–2), 509–529.

Colbo, K., and R. Weller (2007), The variability and heat budget of the upper ocean under the Chile-Peru stratus, *J. Mar. Res.*, *65*, 607–637.

Colbo, K., and R. A. Weller (2009), Accuracy of the IMET sensor package in the subtropics, *J. Atmos. Oceanic Technol.*, *26*, 1867–1890, doi:10.1175/2009JTECHO667.1.

de Szoeke, S. P., and S.-P. Xie (2008), The tropical eastern Pacific seasonal cycle: Assessment of errors and mechanisms in IPCC AR4 coupled ocean atmosphere general circulation models, *J. Clim.*, *21*, 2573–2590, doi:10.1175/2007JCLI1975.1.

de Szoeke, S. P., C. W. Fairall, D. E. Wolfe, L. Bariteau, and P. Zuidema (2010), Surface flux observations on the southeastern tropical Pacific Ocean and attribution of SST errors in coupled ocean-atmosphere models, *J. Clim.*, *23*, 4152–4174.

de Szoeke, S. P., S. Yuter, D. Mechem, C. W. Fairall, C. D. Burleyson, and P. Zuidema (2012), Observations of stratocumulus clouds and their effect on the eastern Pacific surface heat budget along 20°S, *J. Clim.*, *25*, 8542–8567.

Fairall, C. W., E. F. Bradley, J. E. Hare, A. A. Grachev, and J. B. Edson (2003), Bulk parameterization of air-sea fluxes: Updates and verification for the COARE algorithm, *J. Clim.*, *16*, 571–591.

Gentemann, C. L., C. J. Donlon, A. Stuart-Menteth, and F. J. Wentz (2003), Diurnal signals in satellite sea surface temperature measurements, *Geophys. Res. Lett.*, *30*(3), 1140, doi:10.1029/2002GL016291.

Gordon, C. T., A. Rosati, and R. Gudgel (2000), Tropical sensitivity of a coupled model to specified ISCCP low clouds, *J. Clim.*, *13*, 2239–2260.

Gray, A. R., and S. C. Riser (2014), A global analysis of Sverdrup balance using absolute geostrophic velocities from Argo, *J. Phys. Oceanogr.*, *44*, 1213–1229, doi:10.1175/JPO-D-12-0206.1.

Hartmann, D. L., M. E. Ockert-Bell, and M. L. Michelsen (1992), The effect of cloud type on earth's energy balance: Global analysis, *J. Clim.*, *5*, 1281–1304.

Holte, J., F. Straneo, C. Moffat, R. Weller, and J. Farrar (2013), Structure, properties, and heat content of eddies in the southeast Pacific Ocean, *J. Geophys. Res. Oceans*, *118*, 2295–2309, doi:10.1002/jgrc.20175.

Johnson, G. C., and M. J. McPhaden (1999), interior pycnocline flow from the subtropical to the equatorial Pacific Ocean, *J. Phys. Oceanogr.*, *29*, 3073–3089, doi:10.1175/1520-0485(1999)029<3073:IPFFTS>2.0.CO;2.

Johnson, G. C., and K. E. McTaggart (2010), Equatorial Pacific 13°C water eddies in the eastern subtropical South Pacific Ocean, *J. Phys. Oceanogr.*, *40*, 226–236.

Karstensen, J. (2004), Formation of the South Pacific shallow salinity minimum: A southern ocean pathway to the tropical Pacific, *J. Phys. Oceanogr.*, *34*, 2398–2412.

Klein, S. A., and D. L. Hartmann (1993), The seasonal cycle of low stratiform clouds, *J. Clim.*, *6*, 1587–1606.

Large, W. G., and G. Danabasoglu (2006), Attribution and impacts of upper-ocean biases in CCSM3, *J. Clim.*, *19*, 2325–2346.

Lauer, A., K. Hamilton, Y. Wang, V. T. J. Phillips, and R. Bennartz (2010), The impact of global warming on marine boundary layer clouds over the eastern Pacific—A regional model study, *J. Clim.*, *23*, 5844–5863.
Lin, J.-L. (2007), The double-ITCZ problem in IPCC AR4 coupled GCMs: Ocean atmosphere feedback analysis, *J. Clim.*, *20*, 4497–4525.
Locarnini, R. A., A. V. Mishonov, J. I. Antonov, T. P. Boyer, H. E. Garcia, O. K. Baranova, M. M. Zweng, and D. R. Johnson (2010), Temperature, in *World Ocean Atlas 2009, NOAA Atlas NESDIS 68*, vol. 1, edited by S. Levitus, 184 pp., U.S. Gov. Print. Off., Washington, D. C.
Ma, C.-C., C. R. Mechoso, A. W. Robertson, and A. Arakawa (1996), Peruvian stratus clouds and the tropical Pacific circulation: A coupled ocean-atmosphere GCM study, *J. Clim.*, *9*, 1635–1645.
Mechoso, C. R., et al. (1995), The seasonal cycle over the tropical Pacific in coupled ocean atmosphere general circulation models, *Mon. Weather Rev.*, *123*, 2825–2838.
Reid, J. (1973), Transpacific hydrographic sections at Lats. 43°S and 28°S: The SCORPIO expedition. III: Upper water and a note on southward flow at mid-depth, *Deep Sea Res. Oceanogr. Abstr.*, *20*, 39–49.
Rio, M. H., S. Guinehut, and G. Larnicol (2011), New CNES-CLS09 global mean dynamic topography computed from the combination of GRACE data, altimetry, and in situ measurements, *J. Geophys. Res.*, *116*, C07018, doi:10.1029/2010JC006505.
Schneider, W., R. Fuenzalida, E. Rodríguez-Rubio, J. Garcés-Vargas, and L. Bravo (2003), Characteristics and formation of Eastern South Pacific intermediate water, *Geophys. Res. Lett.*, *30*(11), 1581, doi:10.1029/2003GL017086.
Shinoda, T., and J. Lin (2009), Interannual variability of the upper ocean in the southeast Pacific stratus cloud region, *J. Clim.*, *22*, 5072–5088.
Toniazzo, T., C. R. Mechoso, L. C. Shaffrey, and J. M. Slingo (2010), Upper-ocean heat budget and ocean eddy transport in the south-east Pacific in a high-resolution coupled model, *Clim. Dyn.*, *35*, 1309–1329.
Tsuchiya, M., and L. D. Talley (1998), A Pacific hydrographic section at 88°W: Water-property distribution, *J. Geophys. Res.*, *103*, 12,899–12,918, doi:10.1029/97JC03415.
Vecchi, G. A., B. J. Soden, A. T. Wittenberg, I. M. Held, A. Leetmaa, and M. J. Harrison (2006), Weakening of tropical Pacific atmospheric circulation due to anthropogenic forcing, *Nature*, *441*, 73–76, doi:10.1038/nature04744.
Yu, L., and R. A. Weller (2007), Objectively analyzed air sea heat fluxes for the global ice-free oceans (1981–2005), *Bull. Am. Meteorol. Soc.*, *88*, 527.
Zheng, Y., T. Shinoda, G. N. Kiladis, J. Lin, E. J. Metzger, H. E. Hurlburt, and B. S. Giese (2010), Upper-ocean processes under the stratus cloud deck in the southeast Pacific Ocean, *J. Phys. Oceanogr.*, *40*, 103–120.
Zheng, Y., T. Shinoda, J.-L. Lin, and G. N. Kiladis (2011), Sea surface temperature biases under the stratus cloud deck in the southeast Pacific Ocean in 19 IPCC AR4 coupled general circulation models, *J. Clim.*, *24*, 4139–4164.